energies

MDPI

Article

Research on the Formation Characteristics of Fog and Frost on Optical Windows of Unsealed Equipment Compartments in Aircrafts

Chun Shen [1,2], Yuanyuan Liang [1,2], Bo Wei [1,2], Chengchun Zhang [1,3,*] and Tian Zhao [4,*]

[1] National Key Laboratory of Automotive Chassis Integration and Bionics, Jilin University, Changchun 130022, China; shench@jlu.edu.cn (C.S.); liangyy23@outlook.com (Y.L.); weibo21@mails.jlu.edu.cn (B.W.)
[2] School of Automotive Engineering, Jilin University, Changchun 130022, China
[3] Key Laboratory of Engineering Bionics, Ministry of Education, Jilin University, Changchun 130022, China
[4] Beijing Laboratory of New Energy Storage Technology, School of Energy Storage Science and Engineering, North China University of Technology, Beijing 100144, China
* Correspondence: jluzcc@jlu.edu.cn (C.Z.); gszhaotian@126.com (T.Z.)

Abstract: In this study, a numerical method for the formation and dissipation of fog and frost is established using the Eulerian multiphase flow liquid film model. In this approach, the formation and dissipation of fogging and frosting layers is directly determined by the saturation of the water vapor surface, and it does not depend on any empirical coefficients. Additionally, Buck's formula is used to determine the saturation vapor partial pressure, which is applicable for a relatively wide temperature range (−50 °C to 10 °C). This numerical method was validated by the existing experimental data about fogging and frosting, and afterwards the fogging and frosting processes on the optical observation window in the aircraft are further analyzed for three typical working conditions, namely the ground, the fixed-altitude, and the high-altitude descent. The calculation results show that, under the ground working condition, the maximum thickness of the fog layer on the outer surface of the optical window can completely reach the millimeter level within one hour, and the average thickness of the frost layer can reach the sub-millimeter level, which is one order of magnitude smaller compared to under the ground working condition. Under the high-altitude descent working condition, by setting the fixed wall temperature boundary condition on the outer surface of the glass, it is found that in extreme cases, the maximum thickness of the frost layer on the inner wall of the glass can reach the sub-millimeter level within one hour. The research conclusions provide effective basic data support for the subsequent design of anti-fogging and defrosting devices under flight conditions.

Keywords: optical window glass; fogging and frosting; high altitude; temperature and humidity; liquid film model

Academic Editor: Antonio C.M. Sousa

Received: 13 December 2024
Revised: 15 January 2025
Accepted: 17 January 2025
Published: 20 January 2025

Citation: Shen, C.; Liang, Y.; Wei, B.; Zhang, C.; Zhao, T. Research on the Formation Characteristics of Fog and Frost on Optical Windows of Unsealed Equipment Compartments in Aircrafts. *Energies* **2025**, *18*, 437. https://doi.org/10.3390/en18020437

1. Introduction

The problems of fogging and frosting, as well as defogging and defrosting, are commonly found in various transportation systems. They exist not only on the windshields of the cockpits in ground transportation systems like vehicles, but also in crucial positions, such as in the optical windows of the pilot/crew cabins and various avionic equipment cabins in all kinds of aircraft. Once fogging and frosting occur on the observation windows, the transmittance of optical signals will be affected, which will directly lead to the "blindness" of the equipment. Unlike ground transportation vehicles, the equipment compartments of

aircraft have no operators to observe and manually activate the defrosting and defogging equipment. Therefore, it is necessary to predict when fogging and frosting will occur based on the flight operating conditions.

The frosting and fogging processes can be predicted and analyzed by using numerical methods. Under ground conditions, Kim et al. [1] adopted the Computational Fluid Dynamics (CFD) method to predict the frosting situation on the surface of the cold plate and studied the influence of factors affecting the growth of the frost layer, such as the inlet flow velocity, relative humidity, and cold plate temperature. You et al. [2] established a numerical model of the test chamber to predict the heat and moisture distribution caused by air, and investigated the effects of outdoor air temperature, humidity, and wind speed on the fogging state. Yang et al. [3] conducted a simulation of the condensation process inside the carriage based on the Energy and Water Film (EWF) model combined with user-defined functions and found that the temperature, humidity, and mass flow rate of the intake air all have a direct impact on the thickness of the fog layer. Ene et al. [4] established a three-dimensional model of the vehicle cabin at actual scale. They evaluated different air supply temperature of the air conditioner and found that, compared with air at a speed of 6 m/s, introducing air at a speed of 12.5 m/s could reduce the mass flow rate of water-vapor condensation by up to 0.23 g/s. To facilitate the design of automotive air-conditioning systems, Leriche et al. [5] utilized the Star-CCM+ software to construct a fogging model capable of calculating the number of condensed water droplets on the windshield. This model can accurately predict the time and location of fog formation, as well as calculate the size of droplets formed through condensation and the heat and mass transfer processes occurring during the condensation process. Wang et al. [6] established a mathematical model to predict the frosting situation on the aircraft under ground conditions and studied the influence of the aircraft surface temperature, environmental temperature, and relative humidity on the frosting rate of the aircraft.

Under high-altitude conditions, fogging and frosting often occur. The aircraft's thermal insulation materials create a temperature difference between the cold air between the aircraft skin and the insulation layer and the hot air in the warm cabin. This causes the hot air to leak through the thermal insulation materials to the cold surface of the aircraft skin, and, thus, causes the water vapor to condense when it encounters the cold [7]. When the aircraft passes through a cloud, icing occurs on its surface as the supercooled water droplets strike it [8].

There are mainly two methods for defogging and defrosting glass: hot-air heating [9,10] and electric heating [11,12]. At present, most of the research on defrosting and defogging issues focuses on the windshields of automobiles. Kim [13] proposed that vortex generators could be applied to improve the defroster's performance without changing its structure. Kharat [14] established a passenger compartment model using glass, which comprehensively considered the effects of the latent heat and humidity. The study investigated the impacts of different environmental conditions on the in-cabin climate to predict the time required for the fogging and defogging of the windshield to occur. Kitada et al. [15], in order to accurately predict the transient defogging mode of the vehicle's window glass, established a new droplet evaporation/condensation model through an observation of the atomized glass surface and verified its accuracy on a simplified vehicle compartment model and actual vehicles. Tan et al. [16] simulated the transient melting of the frost layer on the front windshield by using the STAR-CCM+ liquid film model and put forward an optimization scheme to increase the surface speed of the front and side windshields. Sandhu et al. [17] used CFD technology to model the defogging system and to assist in the initial design of the defogging and defrosting system, in order to develop a system that can provide a good air flow velocity distribution over the entire windshield.

Currently, CFD simulations of the defrosting process generally model the solid-phase melting region directly, to predict the entire defrosting process [18–20].

Presently, investigations into the phenomena of fogging, frosting, defogging, and defrosting under high-altitude conditions remain conspicuously scarce. It is necessary to establish an analytical method that can reflect the real thermodynamic processes for fog and frost formation under high-altitude flight conditions. In this study, considering Eulerian multiphase flow liquid film model, the numerical method for the formation and dissipation of fog and frost is established. This numerical method can reflect the fog and frost formation under a wide range of temperatures and humidities, from the ground to the high-altitude environment. In this approach, the increase and decrease in fog and frost layer thickness is directly determined by the saturation of the water vapor surface, and it does not depend on any empirical coefficients. Additionally, the application of saturation vapor pressure formulas for a relatively wide temperature range (−50 °C to 10 °C) is discussed. Finally, the simulation analysis is carried out for the typical fogging/frosting working conditions of optical windows, and the effect of the key environmental parameters on the fogging and frosting thicknesses and formation time are elucidated.

2. Numerical Methods and Verification

2.1. Numerical Methods for Fogging and Frosting

In this paper, a coupled heat and mass transfer analysis of the air flow field, liquid film, and solid wall is carried out for the processes of fogging/defogging and frosting/defrosting, as shown in Figure 1. Among them, the air flow field part has a low-speed incompressible internal flow, accompanied by the mass transfer process of water vapor and air, as well as the heat transfer process. It is necessary to solve the continuity equation, momentum equation, energy equation, and component transfer equation. Inside of the liquid film, the mass, momentum, energy, and component transfer processes need to be considered as well. At the interface between the flow field and the liquid film, the phase-change heat and mass transfer processes such as water evaporation, condensation, and solidification need to be considered. For the specific control equations of the calculation model, please refer to the Supplementary Materials.

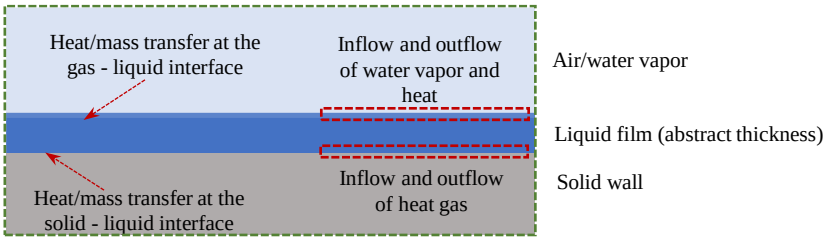

Figure 1. Schematic diagram of the coupled fogging and frosting calculation model of the liquid film, flow field and solid field.

In the numerical simulation in this paper, the commercial CFD software STAR-CCM+ was employed to conduct multi-physical–field coupling calculations for the flow field, liquid film, phase-change process, etc. Leveraging its robust numerical solution capabilities, a high-precision simulation of the interaction process between the gas flow field and the liquid film is carried out. Additionally, in the subsequent analysis, for the aerodynamic heating and cooling effects of the high-subsonic flow field on the outer side of the glass optical window, an equivalent treatment is directly implemented by using the convective heat transfer coefficient.

2.2. Comparison of Water-Vapor-Saturated Pressure Formulas

The water-saturated vapor pressure is the critical value for the conversion of vapor-liquid phase change, which directly affects the condensation rate, and its value is also directly related to the calculation accuracy of the numerical model in Section 2.1. In previous simulation studies on frosting and fogging, the adopted formula for water-saturated vapor pressure only needed to be applicable for the ground temperature conditions (−20 °C to 10 °C). This paper studies the low-temperature conditions (−20 °C to −50 °C) under the high-altitude conditions, and it is necessary to reselect the saturated pressure formula to determine the saturated pressure value under low-temperature conditions. Three saturated partial pressure formulas, namely the Buck formula, the Marti Mauersberger formula and the Antoine equation, are selected and compared with the theoretical value of the saturated pressure at the low temperature [21].

(1) Buck formula

when $T < 0$ °C

$$P_{sat} = 6.1115 \times e^{\frac{(23.036 - \frac{T}{333.7}) \times T}{279.82 + T}} \quad (1)$$

and when $T > 0$ °C

$$P_{sat} = 6.1121 \times e^{\frac{(18.678 - \frac{T}{234.5}) \times T}{257.14 + T}} \quad (2)$$

(2) Marti Mauersberger formula

when $T < 0$ °C

$$\lg P_{sat} = \frac{-2663.5}{T} + 12.537 \quad (3)$$

(3) Antoine formula

$$\lg P_{sat} = 8.07131 - \frac{1730.63}{T + 233.426} \quad (4)$$

where T (°C) is the temperature, and P_{sat} (mmHg) is the vapor-saturated pressure.

As shown in Figure 2, when the temperature is below −20 °C, the values calculated by the Buck and Marti Mauersberger formulas are basically consistent well with the reference theoretical values. When the temperature is above −20 °C, the values calculated by the Buck and Antoine formulas are basically consistent with the reference saturated pressure. In summary, in the entire temperature range from −50 °C to 10 °C, the values calculated by the Buck formula are very close to the theoretical reference values. Therefore, the Buck formula was selected to determine the saturated pressure of water vapor in the subsequent analysis.

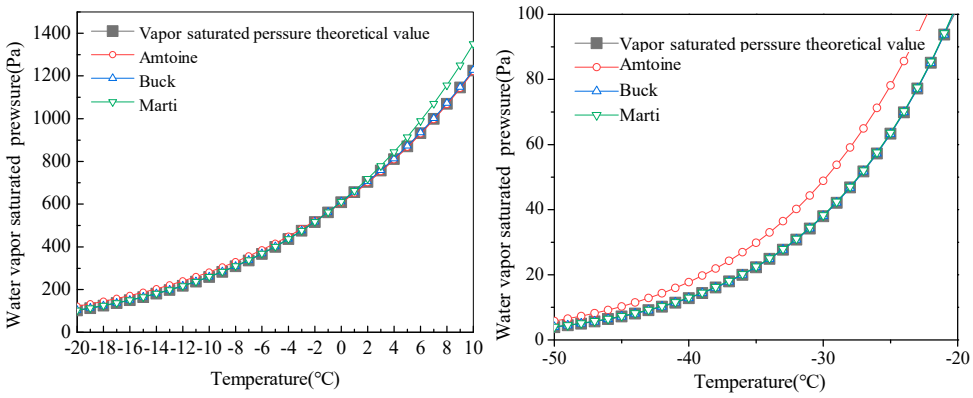

Figure 2. Comparison of the vapor saturated pressure values obtained from the formula and the theoretical approach.

2.3. Experimental Verification of Fogging

(1) Fogging experiment model

The experimental data concerning the mass of the fogging layer from Reference [22] were selected to validate the numerical methods in the Supplementary Materials. The experiments were conducted in a wind tunnel. The ambient temperature was 293.15 K, the humidity was 49.10%, the temperature of the cold surface was 277.45 K, the atmospheric pressure was 91.5 kPa, and the wind speed in the wind tunnel was 1 m/s. The experimental object was a square aluminum flat plate with a size of 5 × 5 cm^2 and a thickness of 3 mm. The experiment lasted for 7.5 h in total, and the mass of the condensed water obtained was 1.8 g. The details of the test apparatus to measure the mass of the fogging layer is shown in Reference [22].

(2) Validation of the numerical method

The computational domain is a cube with a volume of 1 × 1 × 1 m^3. An aluminum plate with the same size of 5 × 5 cm^2 and a thickness of 3 mm is placed at a height of 30 cm from the ground. Its temperature is kept constant at 277.45 K. The ambient temperature is 293.15 K, the humidity is maintained at 49.10%, and the wind speed is 1 m/s. Figure 3 shows the structure and grid schematic diagram of the numerical calculation model. Prismatic layer grids are used to refine the grids at the interface near the solid walls. The trimmed mesh is used to divide the fluid and the solid domain, respectively. The basic size is 10 mm in the fluid region. The prismatic layer grid is used to refine the boundary region close to the aluminum plate. The total thickness of the boundary layer is 2.4 mm, and this boundary layer region includes four layers of equally spaced grids, with the thickness of each layer being 0.6 mm. The total number of grids in the fluid region is about 1.08 million.

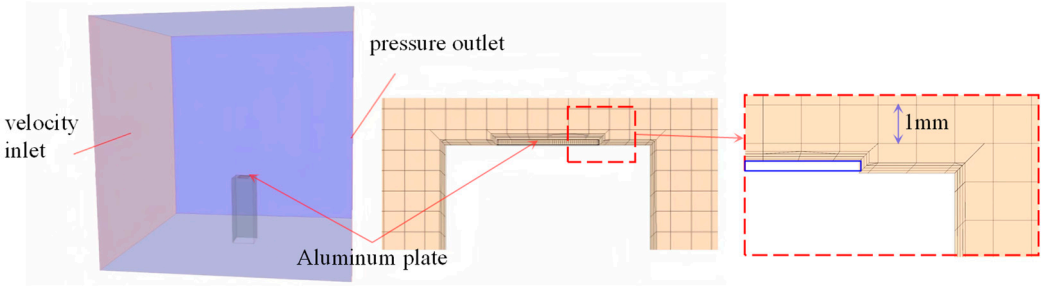

Figure 3. Schematic diagram of the structure and grid of the numerical calculation model.

Figure 4 compares the results between the experiment and the numerical calculation simulation. To reduce the calculation resource consumption, the numerical calculation simulation was carried out for 0.5 h, and a total of 0.12 g of condensed water was obtained. During the experiment, at 0.5 h, the mass of the condensed water obtained was 0.1 g. The slopes of the two lines in the figure represent the condensation rates, and it can be seen that the slopes of the two lines are approximately the same. Through linear interpolation, when the simulation calculation was carried out for 7.5 h, the calculated condensation mass after 7.5 h was (2 × 0.12 g)/h × 7.5 h = 1.8 g, which is consistent with the experimental value. Therefore, it can be considered that the numerical calculation in this paper can reflect the macroscopic process laws of condensation fogging.

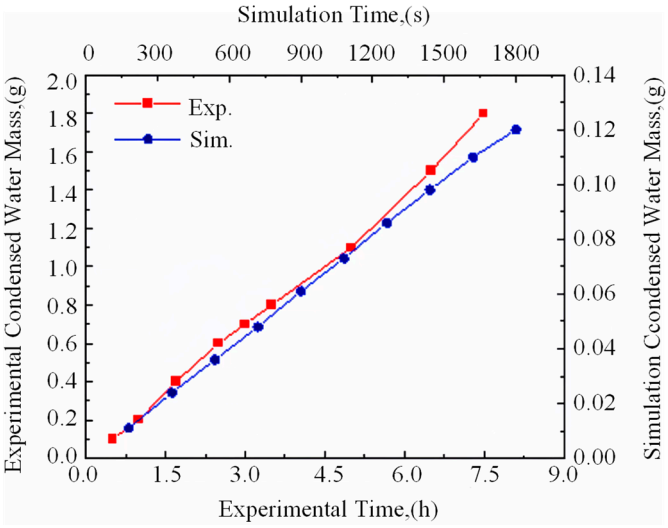

Figure 4. Variation histories of the condensed water mass in the numerical simulation and the experiment [22].

2.4. Experimental Verification of Frosting

(1) Frosting experiment model

The experiment was carried out in a wind tunnel system which consists of a low-temperature environmental chamber, a fan, a humidifier, a flow equalizer and a plexiglass air duct [23]. In the wind tunnel, the ambient temperature was 284.15 K, the humidity was 60%, the temperature of the cold surface was 264.65 K, the atmospheric pressure was 97 kPa, and the wind speed was 0.6 m/s. The size of the aluminum flat plate was 4×4 cm^2 and its thickness was 1 mm. The mass of the frost layer was recorded every ten minutes during the experiment. The experiment lasted for 1.5 h, and the mass of the frost layer reached 1.4 g. The details of the test apparatus used to measure the mass of the frosting layer is shown in Reference [23].

(2) Validation of the numerical method

The computational domain is shown in Figure 2. The left computational domain is a cube with a volume of $1 \times 1 \times 1$ m^3. An aluminum plate with a size of 4×4 cm^2 and a thickness of 1 mm is placed at a height of 30 cm from the ground. Its temperature is kept constant at 264.65 K. The ambient temperature is 284.15 K, the humidity is maintained at 60%, and the wind speed is 0.6 m/s. On the right side is a schematic diagram of the grid of the computational domain for the aluminum plate and its surrounding area. Prismatic layer grids are used to refine the grids at the interface, and their total number is 1.53 million. For the grid of the actual inner cabin computational domain, the cut body grid is also used to divide the fluid and the solid (glass) domains, respectively. The basic size is 4 mm. The prismatic layer grid is used to refine the boundary of the fluid-solid coupling area. The grid size is controlled within 0.25 mm, and the total number of grids increases to 6.15 million.

Figure 5 is a comparison chart of the results between the experiment and the numerical calculation simulation. Six data points within one hour of the experiment are extracted and compared with the simulation data. The simulation results match the experimental results relatively well within the first 40 min. However, the difference between the experimental results and the simulation results gradually increases in the subsequent time. The calculation error is within 20% during the period from 40 min to 60 min.

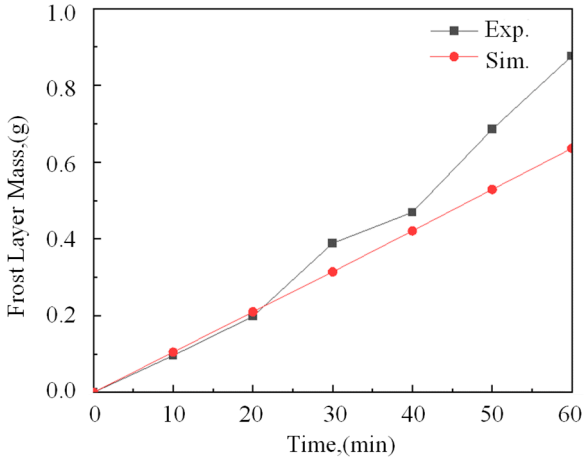

Figure 5. Variation histories of the frost layer mass in numerical simulation and the experiment [23].

Since the experiment reflects real frosting conditions and may be affected by the humidifier, flow equalizer, and other components in the wind tunnel system, the frosting rate fluctuates up and down. However, in the simulation, the relative humidity in the fluid region and the temperature of the aluminum plate are kept constant, so the frosting rate is maintained at a constant level with an unchanged slope. Meanwhile, the density difference between the bottom and the top of the actual frost layer is relatively obvious [23], and it is not taken into account in the numerical model of this paper. The numerical model in this paper does not account for the factor of the frost layer density change, which may also be the reason why the slope of the mass change in the simulation results does not increase.

Anyway, the difference between the calculated results and the actual experimental results in Figure 5 can also reflect the level of errors existing in the numerical simulation on the one hour time order under the ground working conditions. Since the subsequent discussion in this paper mainly focuses on the frosting process, which is also on the one hour time order, the error level in Figure 5 can still be used as a reference.

Therefore, it is considered that the results of the numerical calculation simulation for the frosting match the experimental results quite well, and the numerical frosting model is relatively reliable.

3. Simulation Analysis of Frosting and Fogging on the Optical Window

3.1. Optical Window Cabin Section Model

As shown in Figure 6, the optical window is in the form of a circular optical window, with the thickness of the outer skin being 5 mm. The cut-cell grids are used to divide the fluid domain and the solid (glass), respectively, and the prismatic layer grids are applied to refine the boundary of the fluid–solid coupling area.

The space inside the cabin is 1 m × 1 m × 1 m. The size of the internal observation window box (electronic equipment) is 500 mm × 420 mm × 450 mm (length × width × height), and it is about 50 mm away from the observation window. The size of the hot air device is 445 mm × 140 mm × 150 mm (length × width × height).

The grid of the actual computational domain of the inner cabin also uses cut-cell grids to divide the fluid domain and the solid (glass), respectively, with a basic size of 4 mm. And prismatic layer grids are adopted to refine the boundary of the fluid–solid coupling area, as shown in Figure 7.

(**a**) Optical window geometric model

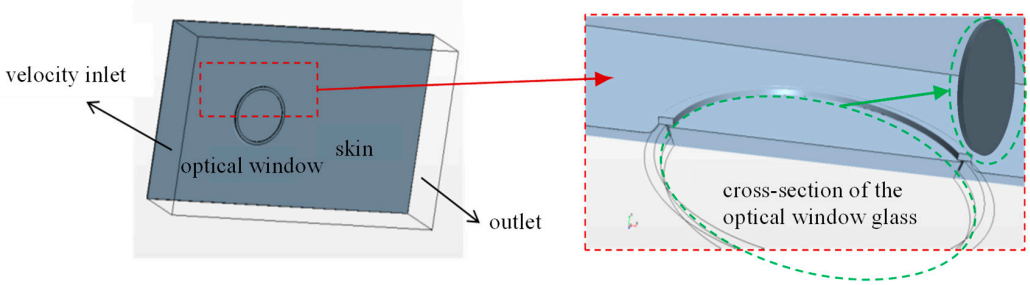

(**b**) Schematic illustration of the computational domain of the simplified model of the inner cabin

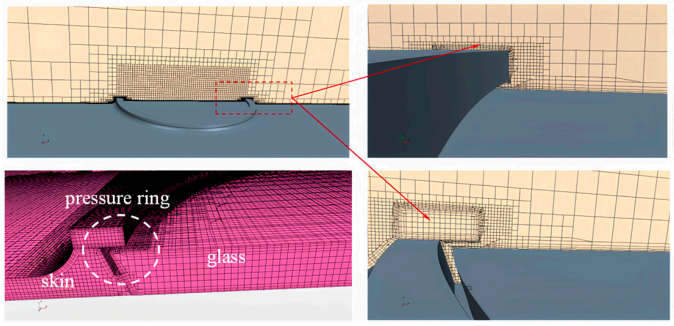

(**c**) Division of the grid area of the internal flow field in the simplified model of the inner cabin

Figure 6. Optical window geometric model and grid.

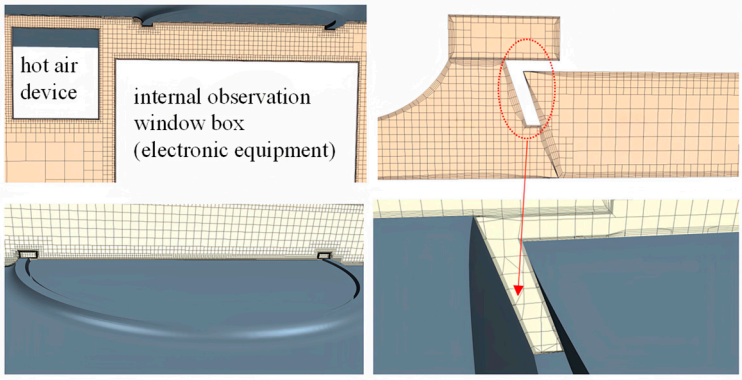

Figure 7. Division of the grid area of the computational domain for the actual inner cabin.

3.2. Boundary Condition

When calculating the ground working condition, as shown in Figure 5, the boundary condition of the left sidewall is set as the velocity inlet with a velocity of 1 m/s. The right sidewall is set as the pressure outlet condition. The two symmetrical sidewalls are set as symmetrical planes. Both the upper and lower surfaces are set as wall conditions.

When calculating the high-altitude working condition, a hot-air device and an internal observation window box (electronic device) are added below the optical window glass in the computational domain of the actual inner cabin. The electronic device is self-heating, with a steady-state power of approximately 150 W, and the heat flux density of each surface is evenly distributed according to the area.

3.3. Grid Independence Verification

The frosting situation under high-altitude conditions is selected as the benchmark case. Grid independence verification is carried out for the grid size of the refined area and the size of the first layer of grid near the wall surface, respectively. Table 1 presents the size of the Mesh0, Mesh1 and Mesh2 at different locations in the computational domain.

Table 1. Grid parameters for Mesh0, Mesh1 and Mesh2.

Mesh	Mesh0	Mesh1	Mesh2
Encryption size of the refined area (mm)	1	2	4
The size of the first layer of grid near the wall surface (mm)	0.1	0.1	0.1
Total number of grids ($\times 10^4$)	1738	720	589

Figure 8 shows the graph of the average frost layer thickness changing over time under different refinement sizes. It can be seen from Figure 7 that the mesh sizes of 4 mm and 2 mm in the encrypted area have little impact on the results. When the mesh size in the encrypted area is reduced to 1 mm, there is a slight difference compared to the results of mesh sizes of 4 mm and 2 mm, but its error remains below 2%, and there is no need to further improve the mesh quality. Since the number of meshes is too large when the mesh size in the encrypted area is 1 mm, the simulation calculation in this paper is carried out based on the mesh with an encrypted size of 4 mm. It should be noted that the corresponding numerical model presented in the Supplementary Materials is based on the macroscopic thermodynamics physical process. Therefore, the macroscopic phenomena for the fogging and frosting layer accumulation are mainly discussed in this paper. The thickness of both the fog and frost layer in Figure 7 is very thin (sub-micrometer level), and it will eventually reach the macroscopic level of sub-millimeter. In other words, the results, at this moment, reflect a relatively short period within the entire macroscopic process, and this paper will not be focusing on the growth mechanism of the frost layer at the microscopic level.

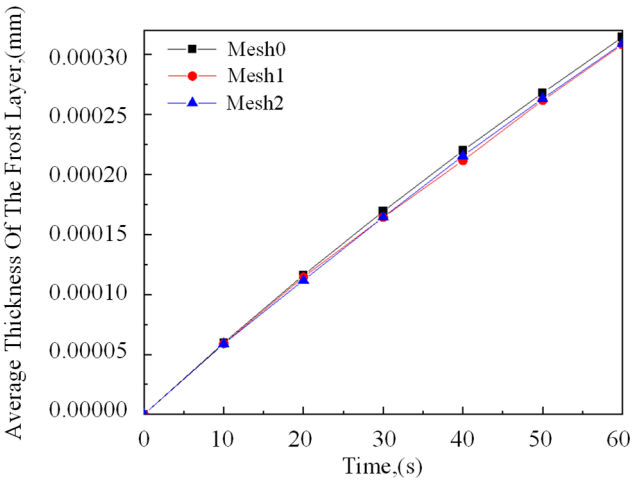

Figure 8. Graph of the change in average frost layer thickness over time under different refinement sizes.

Table 2 shows the size of the Mesh2, Mesh3 and Mesh4 at different locations in the computational domain. Conduct grid-independence verification on the size of the first layer of grid near the wall surface. Set the basic grid size in the refined area to 4 mm and set the size of the first layer of grid near the wall surface to 0.1 mm, 0.2 mm and 0.05 mm, respectively.

Table 2. Grid parameters for Mesh2, Mesh 3 and Mesh4.

Mesh	Mesh2	Mesh3	Mesh4
Encryption size of the refined area (mm)	4	4	4
The size of the first layer of grid near the wall surface (mm)	0.1	0.05	0.2
Total number of grids ($\times 10^4$)	589	589	589

Figure 9 shows the graph of the average frost layer thickness changing over time under different sizes of the first layer of grid near the wall surface. Considering the calculation accuracy and cost, the size of the first layer of grid near the wall surface is selected as 0.1 mm for calculation.

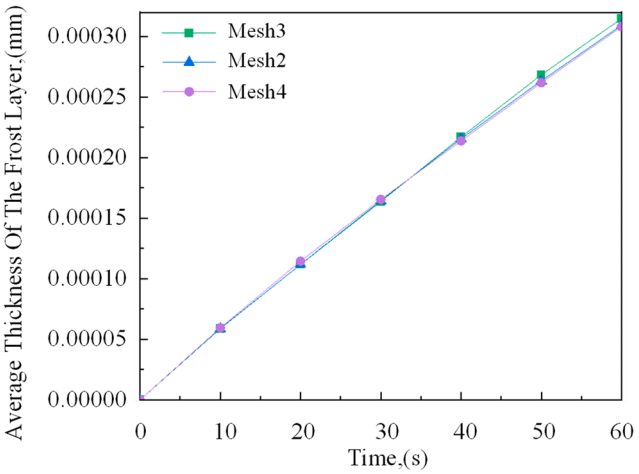

Figure 9. Graph of the change in average frost layer thickness over time under different sizes of the first layer of grid near the wall surface.

3.4. Analysis of the Ground Working Condition

Since there is limited research on frosting under high-altitude conditions in the existing literature, simulation calculations are first carried out for fogging and frosting situations under high temperature and high pressure in the ground condition. This serves as a foundation for the subsequent study of frosting under low temperatures and low pressures at high altitudes.

For the fogging working condition under the ground condition, the external environmental temperature is set at 288.15 K, the relative humidity is 75%, the air pressure value is one standard atmosphere, and the initial temperature of the outer surface of the optical window glass is 288.15 K. The air velocity in the computational domain is 1 m/s. Since it is under the ground working condition, the heating power of the electronic equipment is not taken into account in the calculation.

Figure 10 shows the variation law of the average fog layer thickness on the outer surface of the optical window over time. In the first forty minutes, the condensation and fogging rate is stable. After forty minutes, the fogging rate gradually decreases. This is because the external environmental temperature is higher than that of the optical window glass. After a long period of heat exchange, the temperature of the outer surface of the glass keeps rising, and the corresponding saturated vapor pressure of the water vapor increases with the rise in temperature, reducing the difference between it and the water vapor pressure of the external environment, which leads to a decrease in the condensation rate. The difference between the initial temperature of the glass and the external environmental temperature is small, and so is the difference in water vapor pressure. Even a small fluctuation in the temperature of the outer surface of the glass will have a considerable impact on the condensation rate.

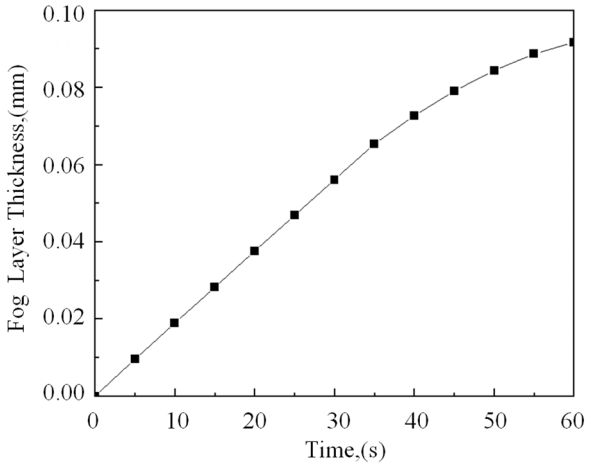

Figure 10. The variation law of the average fog layer thickness on the outer surface of the optical window with time.

Figure 11 shows the variation law of the average frost layer thickness on the outer surface of the optical window over time. The average frost layer thickness gradually increases as time accumulates, and the frosting rate remains stable and essentially does not change over time. Due to the huge difference in the temperature of the outer surface of the glass, the difference in water vapor pressure is also large, so there are significant differences in both the condensation rate and the frost layer thickness. In addition, since the density of frost is smaller than that of liquid water, under the condition of the same mass, the volume of frost is larger. Given that the surface area of the outer surface of the optical window glass is fixed, the difference in thickness is, thus, even greater.

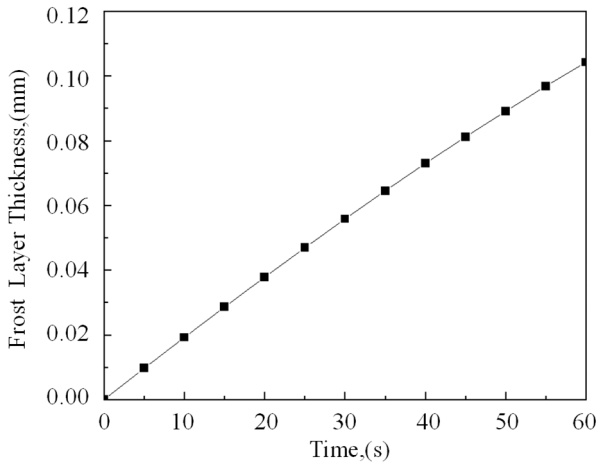

Figure 11. The variation law of the average frost layer thickness on the outer surface of the optical window with time.

3.5. Analysis of the Descent Working Condition at High Altitude

After the aircraft has been cruising at a high altitude for a period of time, the temperature of the optical window glass drops to a relatively low temperature. When the aircraft starts to descend, both the environmental temperature and the relative humidity are constantly rising, and the partial pressure of water vapor on the glass surface is greater than the saturated vapor pressure of water vapor corresponding to the glass temperature. Moreover, since the atmosphere at a high altitude is basically below 0 °C and the cabin section is unsealed, the inside of the it should also be below 0 °C. Therefore, under such conditions, frosting should be the predominant phenomenon.

(1) Influence of cabin temperature

To study the influence of the cabin temperature on the frosting thickness on the surface of the optical window, a situation where the temperature of the optical window drops to 248.15 K when the aircraft is cruising at a high altitude (8000 m) is simulated, and then the frosting situation in autumn and winter, when the aircraft descends to an altitude of 1500 m, is simulated.

Figure 12 shows the variation law of the average frosting layer thickness on the inner surface of the optical window in autumn and winter over time. According to the then literature [24], the atmospheric temperature at an altitude of 1500 m is 288.15 K in autumn and 283.15 K in winter, and the humidity in both seasons is 75%. The frosting layer thickness increases as time accumulates. Since the temperature is higher and the water vapor content is larger in autumn, the frosting layer thickness on the optical window can reach 0.05 mm in one hour. In the winter, the temperature is lower, and the water vapor content is less, so the frosting layer thickness in one hour is 0.04 mm, which is still half the distance from 0.1 mm. As the water vapor pressure gradually decreases, the growth rate of the frosting layer slows down.

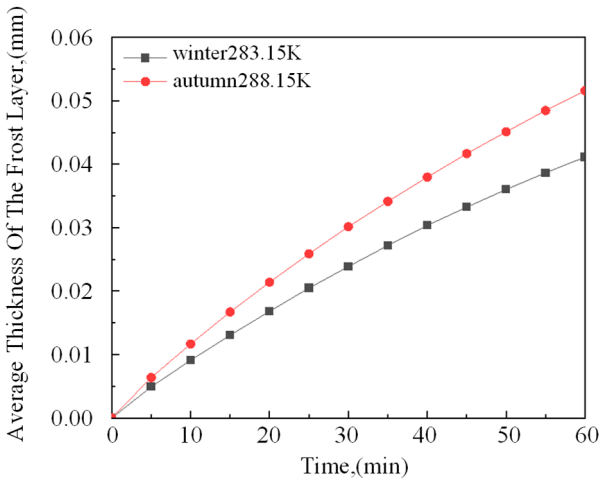

Figure 12. Variation law of the average frost layer thickness on the inner surface of the optical window in autumn and winter over time.

(2) Influence of the optical window temperature

To study the influence of the optical window temperature on the surface frosting, under autumnal conditions (at an altitude of 1500 m), the optical window temperatures were set at 248.15 K and 233.15 K (corresponding to the altitudes of 8000 m and 10,000 m, respectively), and the frosting situations when the aircraft descends to 1500 m after cruising at these temperatures were analyzed.

Figure 13 shows the variation law of the average frost layer thickness on the inner surface of the optical window under different optical window temperatures over time. On average, the frost layer thickness gradually increases as time accumulates. When the optical window temperature is higher, the frosting rate is relatively slower. After one hour of frosting, the average frost layer thickness can exceed 0.05 mm in both cases. The frosting rate basically remains stable and slightly decreases as time accumulates.

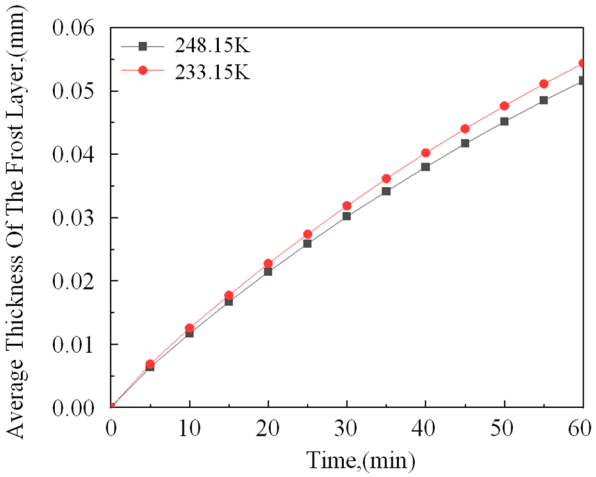

Figure 13. Variation law of the average frost layer thickness on the inner surface of the optical window under different optical window temperatures over time.

(3) Influence of cabin humidity

To study the influence of the cabin humidity on the frosting thickness on the surface of the optical window, under the conditions of spring and autumn, at an altitude of 3000 m (with a temperature of 283.15 K and humidities of 70% and 65%, respectively), the frosting changes after the aircraft descends to 3000 m from cruising at 8000 m are simulated. The results show that the higher the relative humidity is, the more significant the increase in the frost layer thickness will be.

Figure 14 shows the variation law of the average frost layer thickness on the inner surface of the optical window under different relative humidities in spring and autumn over time. The average frost layer thickness gradually increases as time accumulates. Since the relative humidities in spring and autumn only differ by 5%, and the difference in the water vapor pressure value is only about 60 Pa, the influence on the frost layer thickness and the frosting rate is very small. However, when the environmental temperatures inside the cabin are different, the difference in the water vapor pressure is about 360 Pa. In addition, due to the different temperatures, the mass transfer rate is also higher at a higher temperature, so it has a greater impact on the frost layer thickness and the frosting rate.

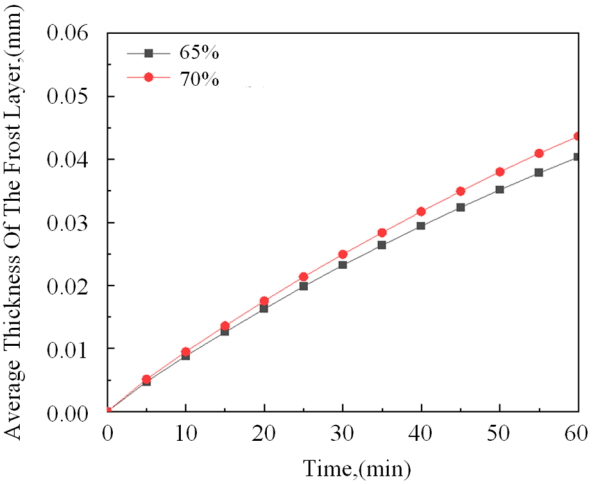

Figure 14. Variation law of the average frost layer thickness on the inner surface of the optical window under different environmental humidities over time.

(4) Influence of the descent altitude

According to the literature [24], two isobaric surfaces of 850 hPa (hectopascal) and 500 hPa are selected for the frosting analysis. The region is southern China and the season is summer. With relatively high temperatures and relative humidities, the frosting phenomenon is more likely to occur. The conditions inside the cabin are consistent with those of the outside environment. The initial temperature of the glass is 237 K, and the heat generated by the equipment is taken into account. In order to obtain the maximum thickness that frosting and fogging can reach under extreme conditions, the thermal boundary condition of the outer surface of the optical window was set as a fixed wall temperature, which is 237 K, the environmental temperature under high-altitude conditions.

Figure 15 shows the graph of the variation of the average frost layer thickness on the glass surface over time, at different altitudes. As the altitude decreases, both the frosting speed and the frosting thickness increase. The water vapor content inside the cabin is constantly decreasing, and the frosting rate gradually decreases over time. When the altitude is 1500 m, the frost layer thickness can reach 0.1 mm. However, when the altitude is 5500 m, due to the limited water vapor content inside the cabin, the magnitude of the frost layer thickness is approximately, or just below, 0.01 mm. Judging from its growth trend, it is very difficult for the frost layer thickness on the glass surface to reach 0.1 mm.

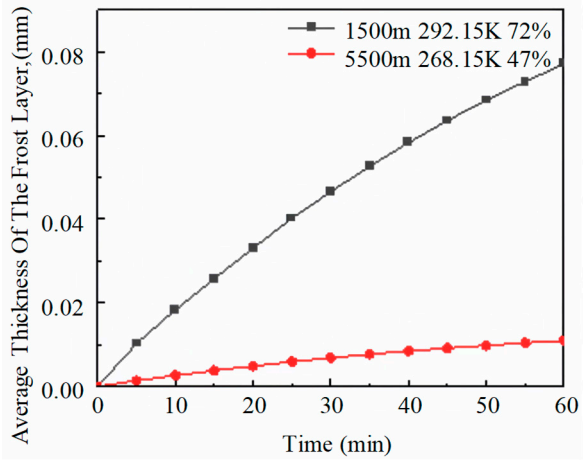

Figure 15. Graph of the variation of the average frost layer thickness on the glass surface over time at different altitudes under the condition of fixed wall temperature.

In the actual situation when an aircraft is cruising at an altitude of 10,000 m, the external environmental temperature is 237 K, and the temperature of the outer surface of the optical window is close to the environmental temperature at the corresponding altitude [25]. When the aircraft rapidly descends to 5500 m or 1500 m, the thermal boundary condition of the outer surface should correspond to the convective heat transfer coefficient and the reference temperature at that altitude, with an initial temperature of 237 K.

The temperature change of the inner surface of the optical window glass is shown in Figure 16. When the aircraft descends to 1500 m, the temperature of the inner surface of the optical window gradually increases due to aerodynamic heating. After about 150 s, the temperature exceeds the freezing point, the frost begins to melt, and fogging occurs. By 240 s, the fog layer reaches a plateau and stops growing, with a thickness not exceeding 0.01 mm. If the aircraft descends to 5500 m, since the environmental temperature of 268.15 K is lower than the freezing point, only frosting occurs, and it gradually stops as the temperature rises.

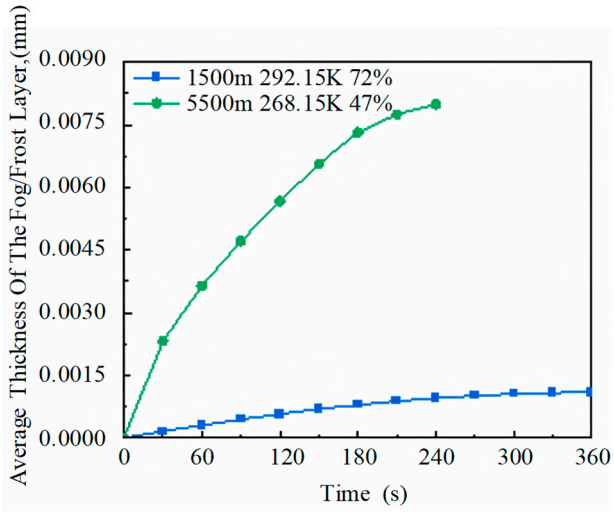

Figure 16. Graph of the variation of the average frost layer thickness on the glass surface over time at different altitudes under the condition of given convective heat transfer coefficient.

4. Conclusions

This paper focuses on the fogging and frosting problems of optical window glass. The numerical simulation method was used to study the formation mechanism of fog and frost under the ground and high-altitude working conditions. Simulation analyses were carried out for three typical fogging/frosting working conditions of optical windows. The fogging and frosting thicknesses as well as the fogging and frosting durations under typical working conditions were obtained. The conclusions are as follows:

(1) Under the ground working condition, the maximum thickness of the fog layer on the outer surface of the optical window can completely reach the millimeter level within one hour, and the average thickness of the frost layer can reach the sub-millimeter level.

(2) Under the working condition of a fixed altitude, as the temperature and humidity inside the cabin increase, the fogging and frosting rates, as well as their thickness, will increase, while as the glass temperature rises, the fogging and frosting rates, as well as their thickness, will decrease.

(3) Under the working condition of high-altitude descent, by setting the fixed wall temperature thermal boundary condition on the outer surface of the glass, it is found that, under extreme conditions, the maximum thickness of the frost layer on the inner wall of the glass can reach the sub-millimeter level within one hour. However, under the thermal boundary condition of the convective heat transfer coefficient found on the outer surface of the glass, it is very difficult to reach the sub-millimeter level.

Supplementary Materials: The following supporting information can be downloaded at: https://www.mdpi.com/article/10.3390/en18020437/s1.

Author Contributions: Conceptualization, C.S.; Methodology, Y.L. and T.Z.; Software, Y.L.; Validation, Y.L.; Formal analysis, Y.L., B.W. and T.Z.; Investigation, B.W.; Data curation, B.W.; Writing—original draft, C.S.; Writing—review & editing, T.Z.; Supervision, C.S., C.Z. and T.Z.; Project administration, C.Z.; Funding acquisition, C.Z. and T.Z. All authors have read and agreed to the published version of the manuscript.

Funding: This research was funded by the National Natural Science Foundation of China (grant numbers 52275289, 52106096, 51875243, 52305306).

Data Availability Statement: The original contributions presented in this study are included in the article/Supplementary Material. Further inquiries can be directed to the corresponding authors.

Conflicts of Interest: The authors declare no conflict of interest.

References

1. Kim, D.; Kim, C.; Lee, K.S. Frosting model for predicting macroscopic and local frost behaviors on a cold plate. *Int. J. Heat Mass Transf.* **2015**, *82*, 135–142. [CrossRef]
2. You, S.; Li, W.; Ye, T.; Hu, F.; Zheng, W. Study on moisture condensation on the interior surface of buildings in high humidity climate. *Build. Environ.* **2017**, *125*, 39–48. [CrossRef]
3. Yang, Y.; Huang, Y.Q.; Zhao, J.S. Optimization of the automotive air conditioning strategy based on the study of dewing phenomenon and defogging progress. *Appl. Therm. Eng.* **2020**, *169*, 114932. [CrossRef]
4. Ene, A.; Catalin, T.; Florin, B.; Georgescu, M. Numerical assessment of the condensation phenomenon on a vehicle's windshield. *IOP Conf. Ser. Earth Environ. Sci.* **2023**, *1185*, 012029. [CrossRef]
5. Leriche, M.; Roessner, W.; Reister, H.; Weigand, B. *Numerical Investigation of Droplets Condensation on a Windshield: Prediction of Fogging Behavior*; SAE Technical Paper Series 2015.10.4271/2015-01-0360; SAE International: Warrendale, PA, USA, 2015.
6. Wang, L.W.; Xu, D.D.; Xing, Z.W. A mathematical model for frost formation on ground aircraft (Conference Paper). *Appl. Mech. Mater.* **2012**, *141*, 147–151. [CrossRef]
7. Norrefeldt, V.; Riedl, G. Investigation of the Impact of a Particle Foam Insulation on Airflow, Temperature Distribution, Pressure Profile and Frost Buildup on the Aircraft Structure. *Aerospace* **2021**, *8*, 359. [CrossRef]
8. Yuan, W.; Yang, Z.; Yan, W.; Zhu, D.; Zhao, N.; Zhu, C. Quantitative Measurement Method for Ice Roughness on an Aircraft Surface. *Aerospace* **2022**, *9*, 739. [CrossRef]
9. Ono, T.; Nagano, H.; Shiratori, S.; Shimano, K.; Kato, S. Analysis of Defogging Performance, Thermal Comfort, and Energy Saving for HVAC System Optimization in Passenger Vehicles. *E3S Web Conf.* **2019**, *111*, 1033. [CrossRef]
10. Rabl, B. Heat pump air conditioning systems for optimized energy demand of electric vehicles. In *SpringerBriefs in Applied Sciences and Technology*; Springer: Cham, Switzerland, 2018; pp. 81–92.
11. Ene, A.E.; Teodosiu, C. Analysis of demisting strategies for electric vehicles. *Sci. Technol. Built Environ.* **2024**, *30*, 87–100. [CrossRef]
12. Lee, S.M.; Lee, J.H.; Bak, S.; Lee, K.; Li, Y.; Lee, H. Hybrid windshield-glass heater for commercial vehicles fabricated via enhanced electrostatic interactions among a substrate, silver nanowires, and an over-coating layer. *Nano Res.* **2015**, *8*, 1882–1892. [CrossRef]
13. Kim, D.; Lee, J.W.; Song, R.; Gim, Y.; Kwon, H.; Ko, H.S.; Lee, J. Improvement of Defogging Performance of Automobile Defroster using Vortex Generators. *Heat Mass Transf.* **2020**, *56*, 2595–2604. [CrossRef]
14. Kharat, R.B.; Nandgaonkar, M.R.; Kajale, S.R.; Ranade, V.V.; Mahajan, S.K. *Modeling of In-Cabin Climate and Fogging of Windshield*; SAE International: Warrendale, PA, USA, 2007.
15. Kitada, M.; Asano, H.; Kataoka, T.; Hirayama, S.; Maruta, Y. *Numerical Analysis of Transient Defogging Pattern on an Automobile*; SAE Technical Papers 2002-01-0223; SAE International: Warrendale, PA, USA, 2002.
16. Libin, T. Computational fluid dynamics simulation and performance optimization of an electrical vehicle Air-conditioning system. *Alex. Eng. J.* **2022**, *61*, 315–328.
17. Sandhu, K.S. Predicting the windscreen demisting performance using CAE. In *Vehicle Thermal Management Systems Conference and Exhibition (VTMS10)*; Woodhead Publishing: Cambridge, UK, 2011; pp. 401–410.
18. Al-abidi, A.A.; Mat, S.B.; Sopian, K.; Sulaiman, M.Y.; Mohammed, A.T. CFD applications for latent heat thermal energy storage: A review. *Renew. Sustain. Energy Rev.* **2013**, *20*, 353–363. [CrossRef]
19. Danaila, I.; Moglan, R.; Hecht, F.; Le Masson, S. A Newton method with adaptive finite elements for solving phase-change problems with natural convection. *J. Comput. Phys.* **2014**, *274*, 826–840. [CrossRef]
20. Kheirabadi, A.C.; Groulx, D. The effect of the mushy-zone constant on simulated phase change heat transfer. Proceedings of the CHT-15. 6th International Symposium on Advances in Computational Heat Transfer, New Brunswick, NJ, USA, 25–29 May 2015.
21. Wexler, A. Vapor Pressure Formulation for Ice. *J. Res. Notional Bur. Stand. A Phys. Chem.* **1977**, *81A*, 5–20. [CrossRef]
22. Tiwari, A.; Kondjoyan, A.; Fontaine, J.-P. Characterization of simultaneous heat and mass transfer phenomena for water vapour condensation on a solid surface in an abiotic environment—Application to bioprocesses. *Appl. Biochem. Biotechnol.* **2012**, *167*, 1132–1143. [CrossRef] [PubMed]
23. Sheng, W.; Lan, Q.Y.; Liu, P.P.; Li, X.L.; Ding, G.L. Experimental Research and CFD Simulation of Frosting on Aluminum Surface. *Fluid Mach.* **2019**, *47*, 83–88. (In Chinese)
24. Gao, H.; Weng, N.Q.; Sun, G.; Zhang, G.Y. Distribution Characteristics of high-altitude temperature and relative humidity in different regions of China. *J. Atmos. Environ. Opt.* **2012**, *7*, 101–107. (In Chinese)
25. Liu, Y.; Dong, S.; Wang, P.; Wang, J. Design of thermal control system for high-altitude and high-speed unmanned vehicle. *Beijing Hangkong Hangtian Daxue Xuebao/J. Beijing Univ. Aeronaut. Astronaut.* **2005**, *31*, 834–838.